Biomedical Optics EXPRESS

Short-coherence off-axis holographic phase microscopy of live cell dynamics

Stefan Witte,[1,2,*] Andrius Plauška,[1,2] Margreet C. Ridder,[3] Laura van Berge,[3] Huibert D. Mansvelder,[4,5] and Marie Louise Groot[2,5]

[1]*These authors contributed equally to this work*
[2]*LaserLaB, VU University Amsterdam, De Boelelaan 1081, 1081 HV Amsterdam, The Netherlands*
[3]*Department of Child Neurology, VU University Medical Centre, 1081 HV Amsterdam, The Netherlands*
[4]*Department of Integrative Neurophysiology, CNCR, VU University, Amsterdam, Netherlands*
[5]*Neuroscience Campus Amsterdam, VU University, 1081 HV Amsterdam, The Netherlands*
**s.m.witte@vu.nl*

Abstract: We demonstrate a single-shot holographic phase microscope that combines short-coherence laser pulses with an off-axis geometry. By introducing a controlled pulse front tilt, ultrashort pulses are made to interfere over a large field-of-view without loss of fringe contrast. With this microscope, quantitative phase images of live cells can be recorded in a full-field geometry without moving parts. We perform phase imaging of HEK293 cells, to study the dynamics of cell volume regulation in response to an osmotic shock.

OCIS codes: (110.0110) Imaging systems; (090.1995) Digital holography; (170.1650) Coherence imaging; (320.7160) Ultrafast technology; (170.1530) Cell analysis.

References and links

1. W. Denk, J. H. Strickler, and W. W. Webb, "Two-photon laser scanning fluorescence microscopy," Science **248**(4951), 73–76 (1990).
2. D. Huang, E. A. Swanson, C. P. Lin, J. S. Schuman, W. G. Stinson, W. Chang, M. R. Hee, T. Flotte, K. Gregory, C. A. Puliafito, and J. G. Fujimoto, "Optical coherence tomography," Science **254**(5035), 1178–1181 (1991).
3. E. Cuche, F. Bevilacqua, and C. Depeursinge, "Digital holography for quantitative phase-contrast imaging," Opt. Lett. **24**(5), 291–293 (1999).
4. U. Schnars and W. P. O. Jüptner, "Digital recording and numerical reconstruction of holograms," Meas. Sci. Technol. **13**(9), R85–R101 (2002).
5. W. Xu, M. H. Jericho, I. A. Meinertzhagen, and H. J. Kreuzer, "Digital in-line holography for biological applications," Proc. Natl. Acad. Sci. U.S.A. **98**(20), 11301–11305 (2001).
6. P. Massatsch, F. Charrière, E. Cuche, P. Marquet, and C. D. Depeursinge, "Time-domain optical coherence tomography with digital holographic microscopy," Appl. Opt. **44**(10), 1806–1812 (2005).
7. G. Pedrini and H. J. Tiziani, "Short-coherence digital microscopy by use of a lensless holographic imaging system," Appl. Opt. **41**(22), 4489–4496 (2002).
8. Z. Wang, I. S. Chun, X. Li, Z.-Y. Ong, E. Pop, L. Millet, M. Gillette, and G. Popescu, "Topography and refractometry of nanostructures using spatial light interference microscopy," Opt. Lett. **35**(2), 208–210 (2010).
9. B. Bhaduri, H. Pham, M. Mir, and G. Popescu, "Diffraction phase microscopy with white light," Opt. Lett. **37**(6), 1094–1096 (2012).
10. E. N. Leith and J. Upatnieks, "Reconstructed wavefronts and communication theory," J. Opt. Soc. Am. **52**(10), 1123–1128 (1962).
11. M. Tziraki, R. Jones, P. M. W. French, M. R. Melloch, and D. D. Nolte, "Photorefractive holography for imaging through turbid media using low coherence light," Appl. Phys. B **70**(1), 151–154 (2000).
12. E. Cuche, P. Marquet, and C. Depeursinge, "Spatial filtering for zero-order and twin-image elimination in digital off-axis holography," Appl. Opt. **39**(23), 4070–4075 (2000).
13. D. Gabor, "A new microscopic principle," Nature **161**(4098), 777–778 (1948).
14. G. Liu and P. D. Scott, "Phase retrieval and twin-image elimination for in-line Fresnel holograms," J. Opt. Soc. Am. A **4**(1), 159–165 (1987).
15. S. Lai, B. King, and M. A. Neifeld, "Wave front reconstruction by means of phase-shifting digital in-line holography," Opt. Commun. **173**(1-6), 155–160 (2000).
16. A. A. Maznev, T. F. Crimmins, and K. A. Nelson, "How to make femtosecond pulses overlap," Opt. Lett. **23**(17), 1378–1380 (1998).

#170691 - $15.00 USD Received 14 Jun 2012; revised 22 Aug 2012; accepted 22 Aug 2012; published 22 Aug 2012

17. Z. Ansari, Y. Gu, M. Tziraki, R. Jones, P. M. W. French, D. D. Nolte, and M. R. Melloch, "Elimination of beam walk-off in low-coherence off-axis photorefractive holography," Opt. Lett. **26**(6), 334–336 (2001).
18. M. C. Ridder, I. Boor, J. C. Lodder, N. L. Postma, X. Capdevila-Nortes, A. Duarri, A. B. Brussaard, R. Estévez, G. C. Scheper, H. D. Mansvelder, and M. S. van der Knaap, "Megalencephalic leucoencephalopathy with cysts: defect in chloride currents and cell volume regulation," Brain **134**(11), 3342–3354 (2011).
19. H. Inoue, S.-I. Mori, S. Morishima, and Y. Okada, "Volume-sensitive chloride channels in mouse cortical neurons: characterization and role in volume regulation," Eur. J. Neurosci. **21**(6), 1648–1658 (2005).
20. Y. Okada, T. Shimizu, E. Maeno, S. Tanabe, X. Wang, and N. Takahashi, "Volume-sensitive chloride channels involved in apoptotic volume decrease and cell death," J. Membr. Biol. **209**(1), 21–29 (2006).
21. W. E. Crowe, J. Altamirano, L. Huerto, and F. J. Alvarez-Leefmans, "Volume changes in single N1E-115 neuroblastoma cells measured with a fluorescent probe," Neuroscience **69**(1), 283–296 (1995).
22. K. Strange, "Cellular volume homeostasis," Adv. Physiol. Educ. **28**(4), 155–159 (2004).
23. B. Rappaz, P. Marquet, E. Cuche, Y. Emery, C. Depeursinge, and P. J. Magistretti, "Measurement of the integral refractive index and dynamic cell morphometry of living cells with digital holographic microscopy," Opt. Express **13**(23), 9361–9373 (2005).

1. Introduction

The ability to visualize dynamic processes at the cellular level is a particularly useful tool in biomedical imaging. Ideally, such a measurement should not influence the process under study. While methods based on nonlinear contrast generation mechanisms [1] have found widespread application, they typically require light intensities where photodamage may become an issue. For single-cell studies, linear optical techniques, which require much lower light intensity, may therefore be preferable.

Two important linear imaging modalities are optical coherence tomography (OCT) [2] and digital holographic microscopy (DHM) [3–5]. In OCT, depth sectioning is achieved through interferometric detection of scattered light emitted by a broadband low-coherence light source. In this case, the depth resolution is determined by the coherence length of the light source instead of the focusing properties of a microscope objective, and can reach the micrometer level. While OCT measures time- or spectral-domain interference at a single point in transverse image space, DHM employs spatial interference between a wide-field image beam and a reference field. DHM is intrinsically a full-field technique, and is fully compatible with the use of high-NA objectives. By using a broadband light source, the OCT coherence gating mechanism can be applied in DHM as well [6,7]. A particularly attractive feature of DHM is that it provides quantitative phase information, enabling tracking of subtle changes in cellular volume and height with high precision [8,9].

Here we combine the advantages of an ultrashort coherence length [6–9] and an off-axis geometry [10,11] into one DHM system, to enable quantitative phase-contrast imaging with sub-cellular resolution. While such a combined system typically suffers from a limited field-of-view [11], we now introduce a novel holographic imaging geometry that provides good overlap of ultrashort pulses crossing at an angle. With this system, a full-field phase-contrast image can be recorded on sub-millisecond timescales, making the technique ideally suited for visualizing cell dynamics. We employ the system to record depth-resolved images of cultured hippocampal neurons and HEK293 cells.

2. Short-coherence off-axis holographic microscopy

In holography, the use of an off-axis (Leith-Upatnieks) geometry [10] is highly beneficial, as it allows easy separation between the interference signal, its complex conjugate and the DC background. This allows direct amplitude and phase retrieval from a single image without twin-image or propagation issues [12], in contrast to an in-line (Gabor) geometry [13] for which more computational effort [14] or multiple images [15] are required. To reduce out-of-plane interference and provide resolution in the axial direction, we employ a light source with an ultrashort coherence length. However, the combination of off-axis holography with broadband coherence gating is hampered by the limited spatial overlap between two ultrashort light pulses crossing at an angle [11], preventing its practical implementation in biological imaging. We circumvent this limitation by generating a reference pulse with a tilted pulse

#170691 - $15.00 USD Received 14 Jun 2012; revised 22 Aug 2012; accepted 22 Aug 2012; published 22 Aug 2012

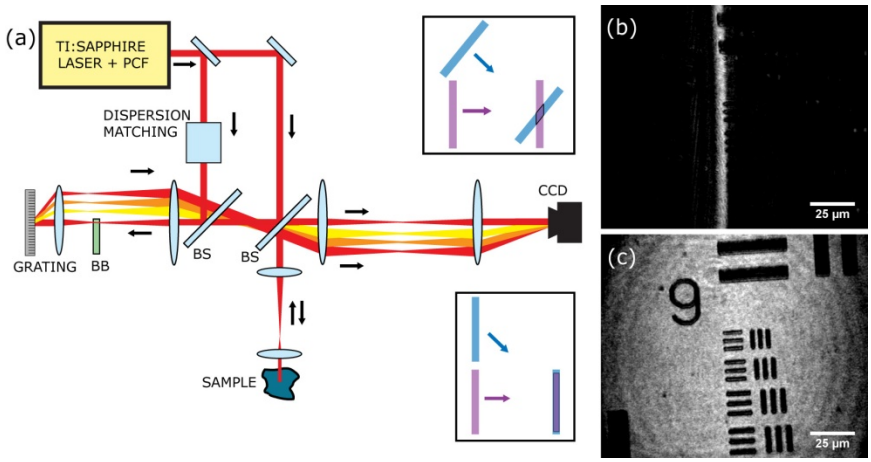

Fig. 1. (a) Setup used for short-coherence off-axis holographic microscopy. A grating in the reference arm introduces a controlled pulse-front-tilt between reference and sample arms, causing short-coherence pulses to overlap over their entire field-of-view despite the finite off-axis angle (lower right inset), in contrast to the normal non-tilted situation (upper right inset). The zero-order reflection is blocked by slightly tilting the grating vertically and placing a beam block (BB) in the returning beam. BS: beam splitter, PCF: photonic crystal fiber, CCD: CCD camera. (b) Hologram of a test sample, measured without pulse front tilt in the reference beam. The limited overlap leads to a strongly reduced field-of-view. (c) Hologram of the same sample, measured with pulse front tilt. A good contrast image is obtained across the entire field-of-view.

front. In contrast to the wavefront, which is always perpendicular to the propagation direction of a wave, the pulse front can have an arbitrary tilt with respect to its propagation direction [16]. This allows precise overlap between two ultrashort pulses in an off-axis geometry over a large field of view (see Fig. 1) [16,17]. The tilted reference pulse is produced by imaging the first order of a diffraction grating onto the CCD camera that records the hologram.

The setup is schematically depicted in Fig. 1(a). The low-coherence light is produced by supercontinuum generation in a photonic crystal fiber with 2.3 µm core diameter (Crystal Fibre A/S), pumped by 4 nJ, 140 fs, 820 nm pulses from a mode-locked Ti:sapphire laser (Coherent Chameleon). The supercontinuum is long-pass filtered to produce a smooth, 150 nm wide spectrum centered at 900 nm, with a coherence length of 2 µm. The microscope is a home-built upright setup using a 40x, 0.8 NA water-immersion physiology objective (Zeiss). To enable holographic imaging, this microscope is placed in one arm of an interferometer. The microscope image plane is relay-imaged onto a 1392x1040 pixel 12-bit CCD camera (Lumenera 3-1M) using f = 20 cm achromatic doublet lenses. For off-axis holography, an angle of 2.4° is introduced between the reference and sample beams at the camera, leading to spatial interference with a period of 26 µm (~4 camera pixels). The sample is imaged in a reflection geometry, where we image the reflection from the microscope slide on which the sample is placed.

The reference arm contains a delay stage for accurate timing of the overlap between reference and sample pulses. A pulse front tilt of 12° is introduced by placing a 300 lines/mm diffraction grating at normal incidence in the beam, and using the first order diffracted beam as the holography reference wave. A 5:1 magnifying telescope images the grating at the image plane of the microscope, ensuring that no spectral smearing is present in the reference beam at the camera position. The telescope magnification also reduces the grating-induced pulse front tilt by a factor 5, matching it to the 2.4° angle between the reference and sample beam. Accurate matching of the pulse front tilt and the angle between the beams is essential to provide good fringe visibility over the entire field-of-view. In our implementation, this matching is conveniently achieved by overlapping the zero-order reflection from the grating

#170691 - $15.00 USD Received 14 Jun 2012; revised 22 Aug 2012; accepted 22 Aug 2012; published 22 Aug 2012

co-linearly with the sample beam, ensuring that the angle between the first-order diffracted beam and the sample beam equals the pulse front tilt induced by the grating. The zero-order reflection from the grating is then blocked during the imaging experiments.

The dramatic improvement in field-of-view (FOV) obtained by pulse-front-tilting is demonstrated in Figs. 1(b) and 1(c), respectively. Figure 1(b) shows the holographic image of a USAF 1951 test target recorded without pulse front tilting, leading to a strong reduction in FOV in the direction of the off-axis angle. In contrast, the pulse-front-tilted reference beam leads to a high-contrast holographic image across the entire FOV, as shown in Fig. 1(c). To obtain a short axial coherence gate, dispersion matching between the reference arms is needed, which we implement by adding a controlled amount of fused silica and BK7 glass to the reference arm. By measuring the image contrast as a function of reference arm length, a coherence gate with a full-width at half maximum (FWHM) of 2.7 μm is found. The transverse resolution is determined to be 0.8 μm using a knife edge technique on the smallest features of Group 7 on the test target.

3. Hologram processing and phase retrieval

After recording a hologram, of which a typical example is shown in Fig. 2(a), it is first Fourier transformed to frequency space. This leads to an image as depicted in Fig. 2(b), where the DC autocorrelation, the off-axis image and its complex conjugate are readily identified. By multiplying everything outside the red circle in Fig. 2(b) with zero, only the image-containing term is retained. The resulting filtered image is inverse Fourier transformed, yielding amplitude and phase of the sample. When needed, 2D phase unwrapping is performed to remove 2π-phase discontinuities. A resulting quantitative phase map of a live, cultured hippocampal neuron is shown in Fig. 2(c).

To optimize image sharpness, numerical refocusing can be performed by multiplying the isolated interference term in the Fourier domain with an additional quadratic phase profile. This feature provides flexibility in imaging range, as any object within the coherence length can be brought into focus, independent of the depth-of-field of the microscope objective.

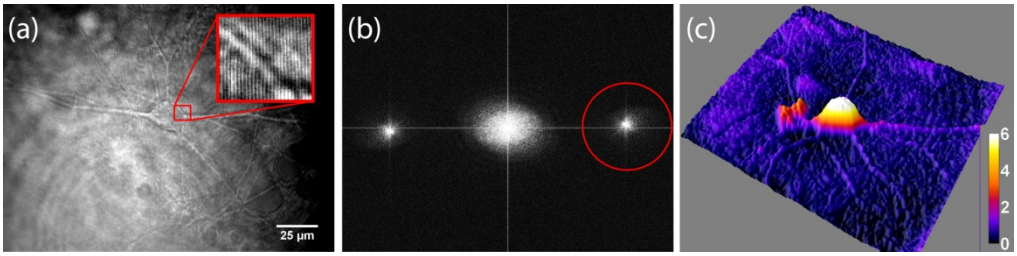

Fig. 2. (a) Single-shot off-axis hologram recorded on the CCD camera. Fine fringes are seen across the entire image. (b) 2D-FFT of the image in (a). The cross-correlation terms containing the electric field information are clearly visible and shifted away from DC because of the off-axis geometry, allowing direct filtering of the area shown in red. (c) Resulting quantitative phase map of a neuron after filtering, inverse 2D-FFT and 2D phase unwrapping.

4. Quantitative phase microscopy of live cell dynamics

Aside from the high-resolution label-free imaging capabilities of off-axis holographic microscopy, the ability to record two-dimensional phase images in a single camera exposure allows for sensitive detection of cellular structural dynamics. We explore this feature by studying HEK293 cells during osmotic stress. The dynamics of cell volume regulation under varying osmotic conditions is a topic of substantial interest, as improper functioning of volume-regulating proteins is involved in various diseases [18,19] and apoptosis [20].

For these experiments, cultured HEK293 cells are plated on coverslips, and placed under the microscope in an extracellular solution containing (in mM): 140 NaCl, 2.4 KCl, 2.0 $CaCl_2$, 4.0 $MgCl_2$, 10 HEPES, 10 glucose, at a total osmolarity of 300 mOsm, and a pH adjusted to

#170691 - $15.00 USD Received 14 Jun 2012; revised 22 Aug 2012; accepted 22 Aug 2012; published 22 Aug 2012

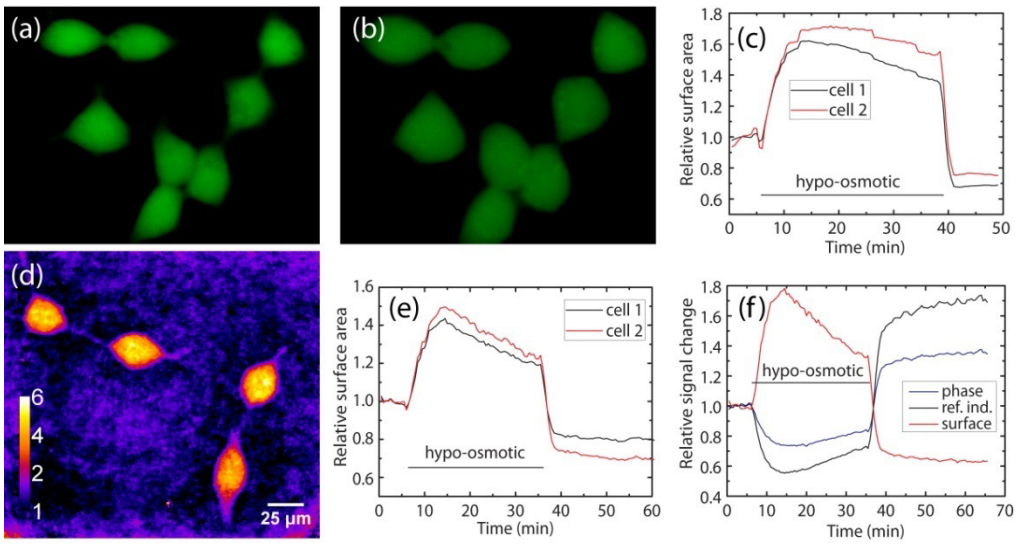

Fig. 3. (a) Fluorescence image of GFP-labeled HEK293 cells under normal conditions. (b) Fluorescence image of the same cells after hypo-osmotic shock, showing cell swelling. (c) Measured surface area of two cells as a function of time during a hypo-osmotic shock, using fluorescence images. (d) Phase microscopy image of unlabeled HEK293 cells. (e) Measured surface area of two cells as a function of time during a hypo-osmotic shock, using phase microscopy. (f) Phase signal and cell surface area as a function of time. When assuming isotropic expansion, an estimate for the refractive index change can be calculated as well.

7.3. An established approach for such measurements is based on fluorescence measurements of cells that have been loaded with green fluorescent dye [21]. We performed such a fluorescence measurement, of which two images are displayed in Fig. 3(a) (under normal osmotic conditions) and Fig. 3(b) (after hypo-osmotic shock), respectively. During continuous image acquisition, the extracellular medium is rapidly diluted to 180 mOsm, causing the cells to swell rapidly due to the outward osmotic pressure. On a timescale of minutes, active volume regulation mechanisms are observed [22]. Finally, the osmolarity is returned to its original value at t = 35-40 minutes by switching back to the original extracellular solution, upon which the cell rapidly shrinks again. Figure 3(c) shows the time evolution of the measured surface area of two fluorescent cells, displaying the rapid swelling upon osmotic shock, the volume regulation phase, and the rapid shrinking when returning to normal osmolarity.

Figure 3(d) shows a typical phase image of unlabeled HEK293 cells measured using our short-coherence off-axis phase microscope. As a direct comparison, we measured the surface area of the cells in a similar way as the fluorescence approach (Fig. 3(e)), yielding similar or better signal-to-noise ratio without the need for labeling. In addition, quantitative phase information is obtained which encodes the optical path length change of the cells (Fig. 3(f)). Even though the cells expand, the phase signal is found to decrease. This effect is readily explained by the fact that upon cell expansion, the refractive index decrease is larger than the geometric height increase, causing the phase signal to decrease [23]. When assuming isotropic volume changes, the geometric changes can be deduced from the surface area measurement, allowing a first-order estimate of the refractive index changes. More advanced decoupling procedures [23] would allow an even better dynamic refractive index measurement.

To control the mechanism underlying active volume regulation, we inhibit the activity of the Cl^- ion channels in the cell membrane by adding Zn^{2+} to the extracellular medium. In many cell types, volume-sensitive outward rectifying Cl^- ion channels have been reported to play a major role in cell volume regulation [19]. Blocking these channels should therefore lead to a strong reduction in cellular volume regulation capability. A phase measurement

#170691 - $15.00 USD Received 14 Jun 2012; revised 22 Aug 2012; accepted 22 Aug 2012; published 22 Aug 2012

under normal conditions is displayed in Fig. 4(a). Directly after the hypo-osmotic shock, the cells undergo active volume regulation, giving rise to a phase signal that exponentially recovers towards its initial iso-osmotic value on the timescale of an hour. A similar measurement with Zn^{2+} ions added to the extracellular medium is shown in Fig. 4(b). In this case, no volume regulation is observed, only passive cell swelling and shrinking due to the osmotic stress remains. These measurements indicate that Cl^- ion channels are indeed involved in active volume regulation in HEK293 cells.

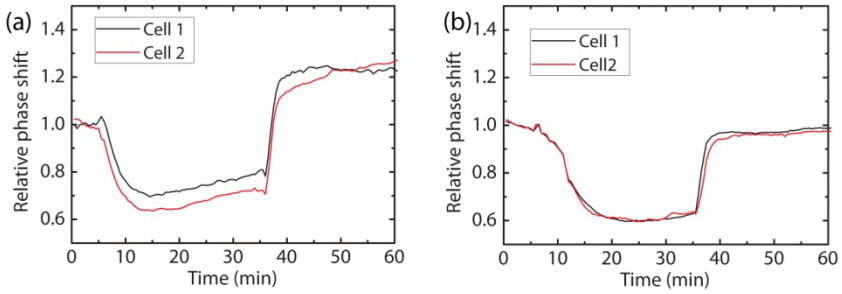

Fig. 4. (a) Measured phase shift during a hypo-osmotic shock using off-axis phase holography on two HEK293 cells. After initial rapid cell swelling, active cell volume regulation is observed. (b) Measured phase shift during a similar hypo-osmotic shock as in (a), but with Zinc added to the extracellular solution. The Zn^{2+}-ions inhibit Cl^- channels in the cell membrane, resulting in an absence of active volume regulation.

5. Conclusions and outlook

In conclusion, we have combined the advantages of short-coherence gating and off-axis holography into a single holographic microscope. To this end, we have developed a novel holographic imaging geometry that introduces a controlled pulse front tilt in the reference beam. Our solution is intuitive and convenient to align. It can readily be implemented on commercial, non-scanning wide-field microscopes, provided that enough room for the reference arm optics is available. The image-plane holography system demonstrated here allows fast switching between conventional bright-field and holographic microscopy, which is highly convenient for alignment purposes.

The use of low-intensity, non-resonant light allows continuous imaging over extended periods of time without loss of contrast or light-induced sample damage. In contrast to fluorescence-based techniques, continuous high-contrast imaging can be maintained over extended measurement times. In addition, the requirements for camera sensitivity and stray light rejection are significantly less stringent. As our system operates with a long-working-distance water-immersion objective, the addition of electrophysiology equipment is relatively straightforward, allowing full integration of physiology techniques with phase-contrast holographic imaging.

With this microscope, we have recorded quantitative phase holograms of unlabeled live cells in a single shot, and studied the dynamics of HEK293 cells during osmotic shocks. We foresee a bright future for this type of holographic phase microscopy for a host of biomedical applications.

Acknowledgments

This work was supported by grants from the Netherlands Organization for Scientific Research (NWO) (917.76.360), Neuroscience Campus Amsterdam and VU University Board. S. W. is supported by an NWO Veni grant (680-47-402).

#170691 - $15.00 USD Received 14 Jun 2012; revised 22 Aug 2012; accepted 22 Aug 2012; published 22 Aug 2012